The Development of a Set of Novel Low Cost and Data Processing-Free Measuring Instruments for Tree Diameter at Breast Height and Tree Position

Linhao Sun [1,2], Zhongke Feng [2,3,*], Yakui Shao [1,2], Linxin Wang [4], Jueying Su [2], Tiantian Ma [1], Dangui Lu [1], Jiayi An [5], Yongqi Pang [2], Shahzad Fahad [1], Wenbiao Wang [6,*] and Zhichao Wang [1,*]

1   Precision Forestry Key Laboratory of Beijing, Beijing Forestry University, Beijing 100083, China
2   Mapping and 3S Technology Center, Beijing Forestry University, Beijing 100083, China
3   College of Forestry, Hainan University, Haikou 570228, China
4   School of Information Science and Technology, Beijing Forestry University, Beijing 100083, China
5   East China Survey and Planning Institute, National Forestry and Grassland Administration, Hangzhou 310019, China
6   Elion Resources Group, Beijing 100026, China
*   Correspondence: zhongkefeng@bjfu.edu.cn (Z.F.); wangwenbiao@elion.com.cn (W.W.); zhichao@bjfu.edu.cn (Z.W.)

Abstract: In current forestry investigation studies, the research hotspots have tended to concentrate on ascertaining the precision of certain tree parameters. This has resulted in an augmented intricacy of the technique in terms of algorithms and observation instruments. The complexity of the technology and the cost of the equipment make it impossible to use for large-scale forest surveys, for example, a national forest inventory (NFI). The aim of our study was to design a new type of low-cost measuring method that could be utilized in a NFI and in developing countries. Meanwhile, the newly designed method was expected to be able to output certain forest measurement factors without necessitating data processing by NFI field investigators. Based on these objectives, we developed a measuring method that included hardware comprised of two tools. The first tool was an electronic measuring tape that contained a microcontroller unit (MCU) and could automatically record and collaborate with other equipment via wireless protocols. The second tool was a tree stem position mapper that utilized our own designed mechanisms. The results showed that the tree DBH measurements exhibited a 0.05 cm (0.20%) bias and a 0.36 cm (1.45%) root mean square error (RMSE), and the biases on the x-axis and the y-axis of the tree position estimations were −15.92–9.92 cm and −25.90–10.88 cm, respectively, accompanied by corresponding RMSEs of 15.27–29.40 cm and 14.49–34.68 cm. Moreover, an efficiency test determined that the average measurement time per tree was 20.34 s, thus, demonstrating a marked improvement in speed by nearly one-fold compared to the conventional method. Meanwhile, this measurement kit costs less than 150 Euros and is economically suitable for large-scale applications. We posit that our method has the potential to serve as a standard tool in a Chinese NFI and in developing countries in the future.

Keywords: forest surveying method; diameter at breast height; tree position; tunnel magnetoresistance encoder; ultra-wideband technology

1. Introduction

1.1. Our Aims

Trees are essential to the health of our planet, as they provide oxygen, sequester carbon dioxide, and form a major part of the global carbon cycle. Not all trees are found live in rich and developed nations; the world we live in comprises many countries with varying levels of development. In fact, a large percentage of the world's trees are found in the world's poorest countries, often in the most difficult environmental conditions. This presents a unique challenge to those seeking to conserve, protect, and manage these forests.

Tree measuring instruments provide us with the fundamental knowledge of trees. To address the inequality among countries, a new measuring instrument must be developed that can be used by people from all levels of development. This new instrument should be affordable, reliable, and easy to use, and should allow users to accurately measure and protect their trees. The aim of this study was to explore how to construct a set of new measuring instruments with a relatively low cost, while still achieving a performance level similar to that of higher-valued measuring instruments. We would, therefore, like every tree in the world to be observed using similar technical criteria via a forest field survey. The development of standardized observation and assessment methods would enable researchers to gain a better understanding of forests on our planet.

1.2. Technical Review

Accurate and efficient acquisition of tree diameter at breast height (DBH) and tree position are of great significance in forest resource inventories and sustainable forest management [1–3]. Tree DBH, measured at a height of 1.3 m, is essential to estimate other tree characteristics such as tree height, basal area, volume, and tree growth, [4–6]; tree position is helpful for evaluating stand density, revealing the relationships between trees and tree species, and predicting population development trends [7–9]. Tree DBH is usually measured manually with a diameter tape or a caliper [10,11]. Traditional tree position measurements use a forest compass equipped with tapes or a total station [1,8,12]; however, these tools and methods are not convenient, time-consuming, labor-intensive, and inefficient, and may increase mistakes in measurement and data entry [13–15]. Therefore, developing a convenient, accurate, and efficient method for tree DBH and tree position measurements has become an important component of precision and modern forestry [16–19].

During the last three decades, many forest surveying methods have been proposed [1,7,12–14]. From the traditional forest inventory to modern solutions and practices, new measurement methods using electronic tools, wireless sensors, and the Internet of Things (IoT) are gradually being applied [11,20–23]. These methods can be divided into two categories: contact methods and non-contact methods [24–26]. Contact methods are usually only applied to tree DBH measurements, allow for the highest accuracy [7,9,11,24–26], and require equipment such as an electronic tree measuring fork [11], an electronic bar [27], a draw-wire displacement sensor [28,29], and an electronic caliper using a capacitive gate sensor [30]. Meanwhile, non-contact methods for tree DBH or tree position measurements and involve techniques such as close-range photogrammetry (CRP) [25,26], terrestrial laser scanning (TLS) [31–36], machine vision or simultaneous localization and mapping (SLAM) using a smart phone [1,13,37], and the use of global positioning system (GPS) or global navigation satellite system (GNSS) devices [38–41]. However, these non-contact methods can easily be affected by the field investigation environments such as stand density, abundance of shrubs and vegetation, and intensity of illumination. Hence, non-contact methods are expensive to operate in terms of computation time. Furthermore, they necessitate considerable computational resources, complex data processing techniques, and expensive equipment, and many are not easily transportable due to their size and weight. Therefore, many practical and technical restrictions on accuracy, precision, operational simplicity, time, equipment portability, and cost still exist for applying these methods in forest inventories.

The development of digital forestry is imperative to obtain a high-precision, low-cost, efficient and integrated forest surveying system to overcome the time-consuming and labor-intensive nature of traditional field surveys. Recent developments in sensor and electronic technology make this possible. Magnetic rotary encoders that possess a sine-cosine relationship with the shaft angle are widely used in modern industry, as well as automobile, aircraft, and electronic products [42,43]. According to technical principles, these encoders can be divided into four types: hall-effect, anisotropic magnetoresistance (AMR), giant magnetoresistance (GMR), and tunnel magnetoresistance (TMR) [42–46]. As the newest magnetic sensing technology, a TMR encoder has more advantages than the other three types of encoders, such as high sensitivity, high magnetic field resolution, fast

response time, good temperature drift characteristics, low power consumption, and small size [42–47]. Therefore, a TMR encoder is very suitable for developing a portable high-precision device for measuring tree DBH [47]. The ultra-wideband (UWB) technology is based on sending and receiving carrier-less radio impulses using extremely accurate timing, and it is used in indoor localization of moving objects in complicated, light to medium sheltered, and space-constrained environments [48–50]. Compared with other wireless technologies such as Wi-Fi, Bluetooth, and ZigBee, it has higher precision, better anti-interference ability, stronger penetration ability, and wider communication range [51–53]. Therefore, this technology is particularly suitable for measuring distance and positions in forests. Zhao et al. [23] developed a new UWB positioning measurement tool to estimate tree positions; however, similar to other indoor UWB positioning methods, they all required setting up at least four UWB modules for anchors at four corners and one UWB module as a tag. Additionally, in order to calculate the position of the UWB tag, surveyors must obtain the three-dimensional (3D) coordinate positions of the UWB anchors before each sample plot measurement. This preparatory work is also time-consuming and complicated in forest surveys.

In this paper, we propose a new integrated forest surveying method that combines the measurement of tree DBH and tree position using accurate, efficient, portable, and low-cost hardware and rapid, non-complex, and high-resolution measurement algorithms for tree DBH calculations and tree position estimations. We developed a handheld device and a UWB base station to form the hardware, which was mainly based on a TMR encoder, UWB technology, and multi-sensors. Moreover, as a collaborator with the hardware, we further developed the workflow and software with the functions of measurement, recording, uploading, and storing tree DBH and tree position data, which would greatly reduce the labor intensity required for a forest survey.

2. Materials and Methods

2.1. Study Area

The experiment was performed in Beijing Olympic Forest Park (39°50′ N, 116°24′ E), Beijing, China (Figure 1). We sampled 6 circular plots (706.86 m^2) with a diameter of 30 m. The basic descriptions of the plots are shown in Table 1.
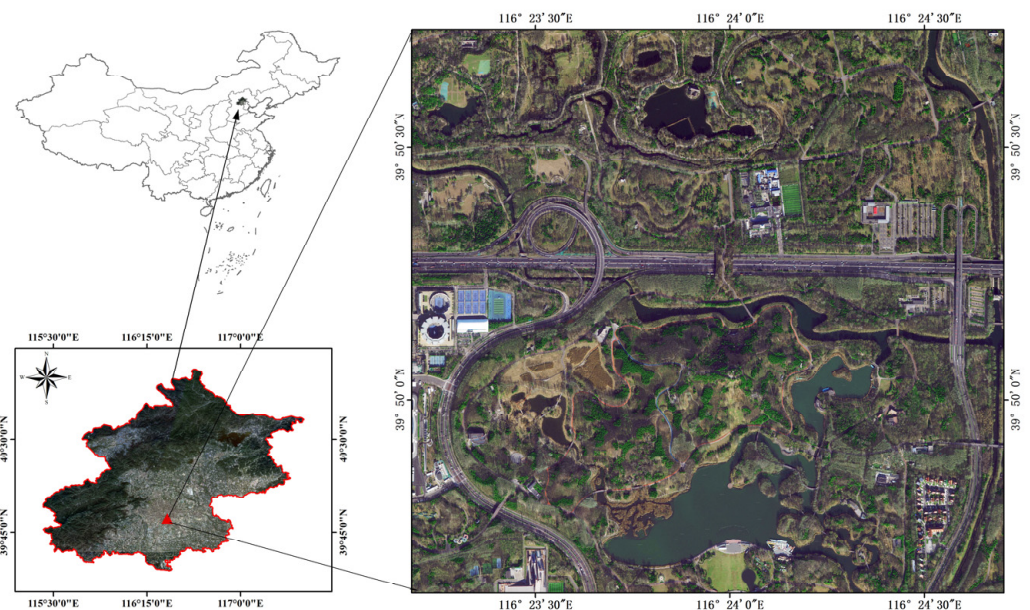

Figure 1. Location of the study area.

Table 1. Descriptive statistics of the plots.

Plot	Number of Trees	Dominant Species	DBH (cm)		
			Mean	Min	Max
1	43	*Ginkgo biloba* L.	21.67	14.6	31.2
2	51	*Salix matsudana Koidz*	22.26	14.3	28.8
3	46	*Ginkgo biloba* L.	19.62	14.2	32.7
4	41	*Populus tomentosa*	30.93	11.9	43.5
5	40	*Salix matsudana Koidz*	19.92	13.7	27.5
6	43	*Populus tomentosa*	27.88	14.4	48.9

2.2. Methods

2.2.1. Hardware for Measuring Tree DBH and Tree Position

The hardware for measuring tree DBH and tree position mainly consisted of a hand-held device (weight 293 g and price USD 80), a base station (weight 2092 g and price USD 280), and a supporting tripod (weight 1263 g and price USD 30), with a total weight of 3648 g and a total price of USD 390, as shown in Figure 2. The handheld device was mainly composed of a tape, keys, a handle, a touch screen, a UWB tag, and other built-in electronic and mechanical components (a TMR encoder, a printed circuit board, and so on, as shown in Section 2.2.3), as shown in Figure 2b. The printed circuit board was designed using the LICHUANG-EDA software, and embedded with an altimeter, power module, a micro-controller unit (MCU), a secure digital memory card (SD card), Bluetooth, and circuit interfaces. The basic descriptions of the handheld device's electronic components are listed in Appendix A (Table A1). The base station consisted of an electronics box, a mobile battery, and three 1.35 m long poles (interval 120°) with a UWB module, a fixing knob, a folding connector, and two carbon fiber rods, as shown in Figure 2c. The electronics box was mainly composed of a 3D electronic compass to obtain attitude angles (roll, pitch, heading, as shown in Section 2.2.4). The basic descriptions of the base station's electronic components are listed in Appendix B (Table A2). The three poles and tripod could be folded and shrunk, which facilitated survey crews in the field with carrying the base station, as shown in Figure 2a,c. During measurements, the handheld device could measure tree DBH and altitude data alone, and the distances between the tag and three anchors were obtained through cooperation with the base station.

2.2.2. The Measurement Workflow

Figure 3 presents the workflow for measuring tree DBH and tree position in a plot. The measurement workflow was as follows:

(1) The base station, equipped with a supporting tripod, was placed in the center of the plot, and then the handheld device and base station were used to obtain initial data from a 3D compass and an altimeter.

(2) Each tree was measured as follows: First, the surveyor walked to the tree with the handheld device. Second, the tape of the handheld device was pulled out around the stem at breast height. Third, the surveyor pressed the keys to record the tree DBH and tree position data.

(3) Once the measurement process was finished, the data were automatically uploaded to a mobile phone. Then, the equipment was packaged and awaited transfer to the next sample plot.
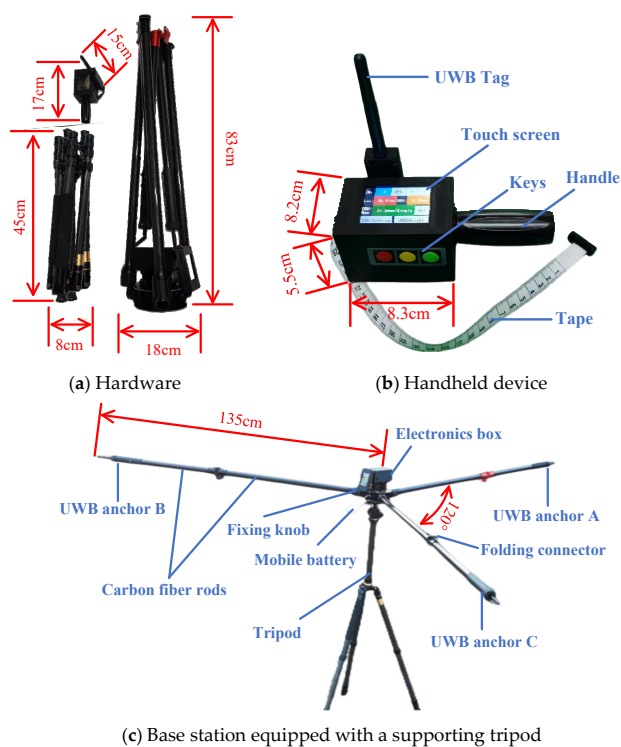
(**a**) Hardware

(**b**) Handheld device

(**c**) Base station equipped with a supporting tripod

Figure 2. The hardware for measuring tree DBH and tree position.
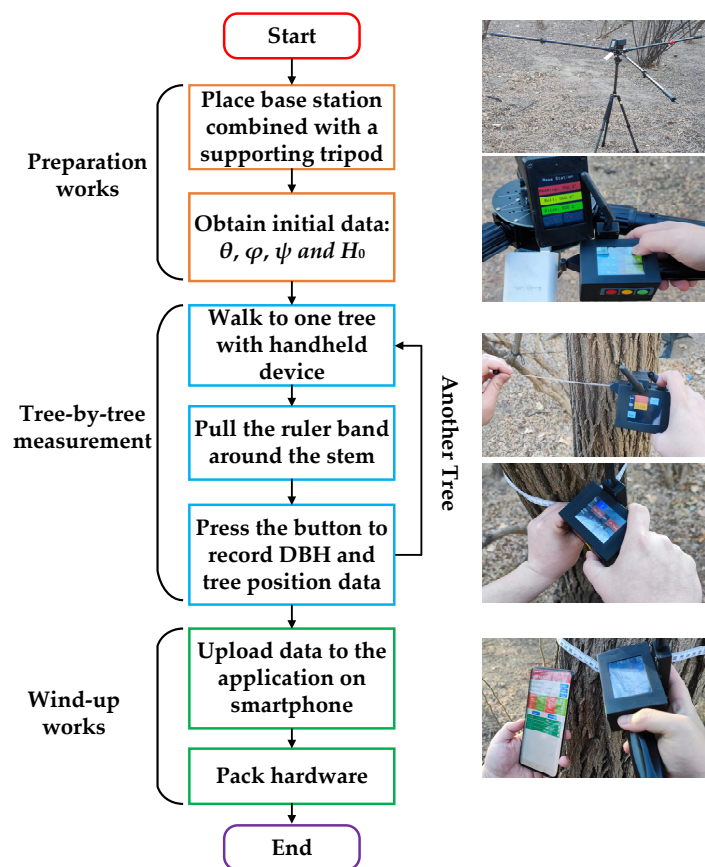

Figure 3. The workflow for measuring tree DBH and tree position in a plot.

2.2.3. Measurement Algorithms for the Tree DBH Calculations

Figure 4 presents the internal structure and the tree DBH measurement principle of the handheld device. When the tape is pulled out, the turntable drives the flange to rotate at the same time. Furthermore, the flange drives the bearings of the TMR encoder to rotate simultaneously. Therefore, rotational information of the turntable can be sensed by the TMR encoder, such as encoding of a single cycle and the cumulative value of the rotational number of the turntable. Assume that encoding of a single cycle is *CN* and the cumulative value of the rotational number of the turntable is *TN*. *CN* from 0 to 8191 corresponds to the rotation position of the turntable from 0° to 360° in one rotation. *TN* equals the cumulative value of the increased or decreased number of rotations of the turntable under the action of the ruler belt pulling out or the spring recovery. According to the principle of a TMR encoder (Appendix C), we designed a tree DBH calculation program in the MCU (Figure 5). When the turntable rotates clockwise (CW), the DIR port of the TMR encoder outputs a low-level signal to the voltage detection port of the MCU, and when it rotates counterclockwise (CCW), the DIR signal is high. If the external interrupt INT0 port of the MCU detects a rising or a failing edge signal from the STEP port of TMR encoder, *CN* adds one or subtracts one between 0 and 8191, depending on whether the DIR signal is high or low, accordingly (blue rectangle in Figures 4 and 5a). If the external interrupt INT1 port of the MCU detects a failing edge signal from the INX port of TMR encoder, *TN* also adds one or subtracts one depending on whether the DIR signal is high or low, accordingly (blue rectangle in Figures 4 and 5b). After obtaining *CN* and *TN*, the tree DBH can be calculated by the MCU (Figure 5c).
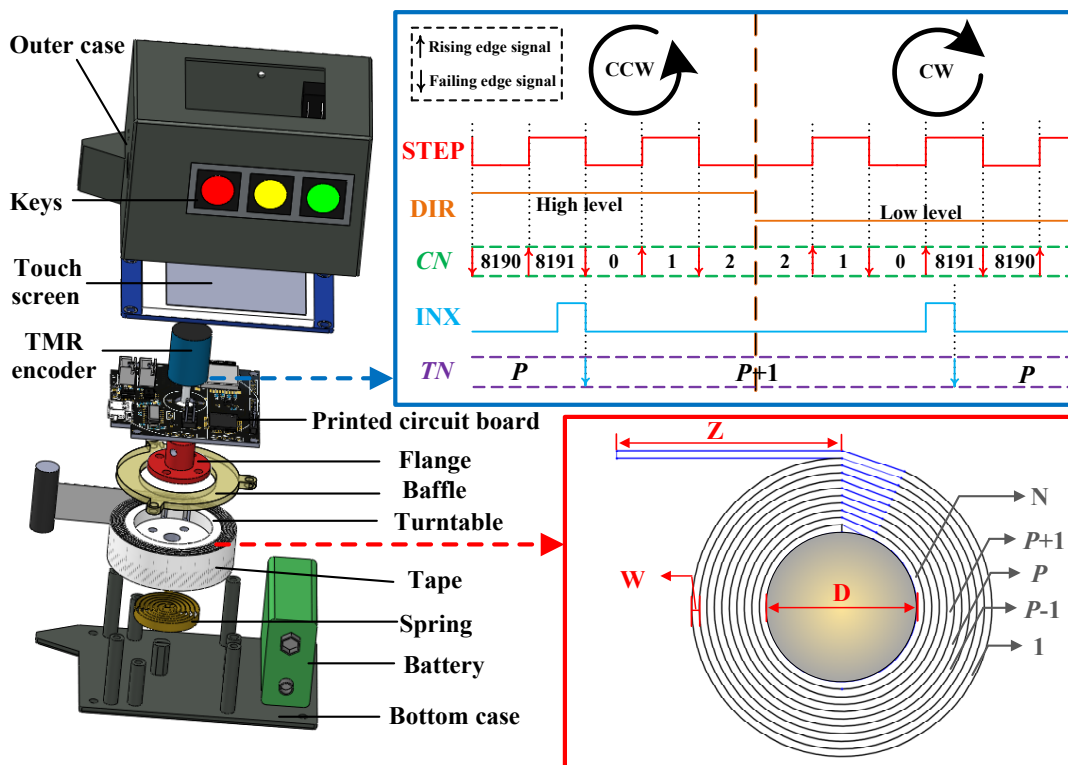

Figure 4. Internal structure and the tree DBH measurement principle of the handheld device. Blue rectangle, the timing of electrical signals diagram output by the TMR encoder to the MCU. Red rectangle, top view of the turntable and the tape.
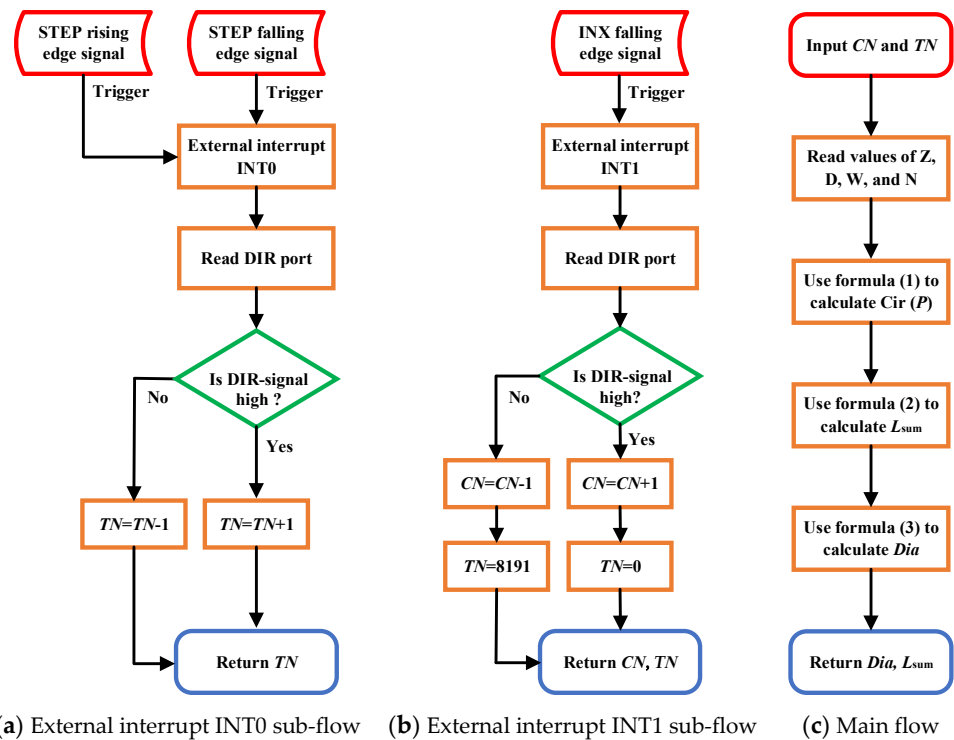
(**a**) External interrupt INT0 sub-flow   (**b**) External interrupt INT1 sub-flow   (**c**) Main flow

Figure 5. Flow chart of the tree DBH calculation program in the MCU.

In order to obtain the value of the tree DBH, the circumference of the tape for each rotation is needed (red rectangle in Figure 4), which can be calculated using the following formula:

$$\text{Cir}(P) = \left[\text{W}(\text{N} - P + 1) + \frac{\text{D}}{2}\right] \cdot \left[2\pi - \arccos\frac{\text{D}}{2\text{W} + \text{D}} + \sin\left(\arccos\frac{\text{D}}{2\text{W} + \text{D}}\right)\right] \quad (1)$$

where P is the current number of rotations of the turntable, N is the maximum number of rotations of the turntable, W is the width of the tape, and D is the diameter of turntable.

Then, Cir (P) can be used to calculate the length of the tape on the outside of handheld device, using the following formula:

$$L\text{sum} = \sum_{P=1}^{TN-1} \text{Cir}(P) + \frac{\text{Len}(TN) \cdot (CN + 1)}{8192} + \text{Z} \quad (2)$$

where Z is the length of the exposed part of the tape, CN is the encoding of a single cycle obtained by the MCU; TN is the cumulative value of the rotational number of the turntable obtained by the MCU.

Finally, the DBH can be calculated using the following formula:

$$Dia = L\text{sum}/\pi \quad (3)$$

2.2.4. Measurement Algorithms for the Tree Position Estimations

In order to obtain a tree's position in a plot, the spatial coordinates of three anchors are first calculated by using the attitude angles from the 3D electronic compass after the three poles of the base station are unfolded (Figure 6).
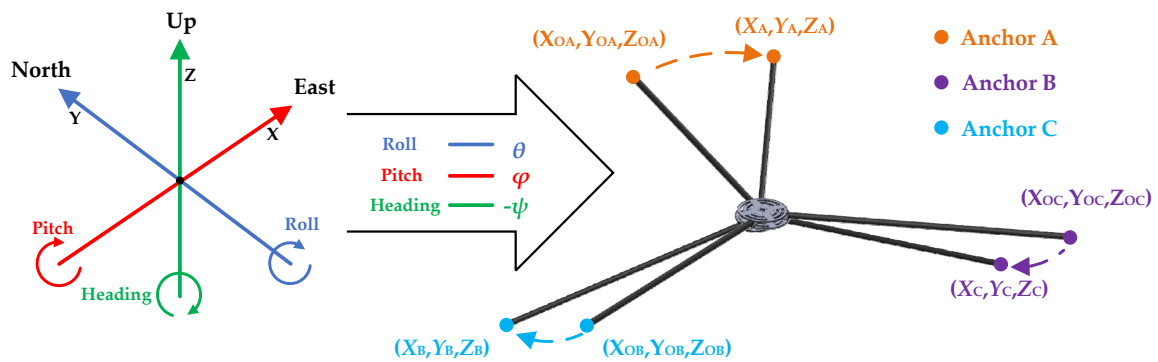
Figure 6. Calculate the coordinates of the three anchor points.

The spatial coordinate of Anchor A can be obtained as shown in Equation (4). By the same token, the spatial coordinates of the two other anchors can be obtained.

$$\begin{bmatrix} X_A \\ Y_A \\ Z_A \end{bmatrix} = \begin{bmatrix} \cos\theta & 0 & -\sin\theta \\ 0 & 1 & 0 \\ \sin\theta & 0 & \cos\theta \end{bmatrix} \begin{bmatrix} 1 & 0 & 0 \\ 0 & \cos\phi & \sin\phi \\ 0 & -\sin\phi & \cos\phi \end{bmatrix} \begin{bmatrix} \cos\psi & -\sin\psi & 0 \\ \sin\psi & \cos\psi & 0 \\ 0 & 0 & 1 \end{bmatrix} \begin{bmatrix} X_{OA} \\ Y_{OA} \\ Z_{OA} \end{bmatrix} \quad (4)$$

where θ is the angle of roll; ϕ is the angle of pitch; $-\psi$ is the angle of heading; (X_A, Y_A, Z_A), (X_B, Y_B, Z_B), and (X_C, Y_C, Z_C) are the spatial coordinates of Anchor A, Anchor B, and Anchor C, respectively; (X_{OA}, Y_{OA}, Z_{OA}), (X_{OB}, Y_{OB}, Z_{OB}), and (X_{OC}, Y_{OC}, Z_{OC}) are the original spatial coordinates of Anchor A, Anchor B, and Anchor C, respectively, when $\theta = 0$, $\phi = 0$, and $-\psi = 0$.

After obtaining Z_A, Z_B, and Z_C, the 3D scalars H_1, H_0, Dis_A, Dis_B, and Dis_C are transformed into two-dimensional (2D) scalars in the OXY plane, as shown in Figure 7. Dis_A, Dis_B, and Dis_C are the linear distances between the tag and Anchor A, Anchor B, and Anchor C, respectively, in the 3D coordinate system. The principles of calculating Dis_A, Dis_B, and Dis_C are given in Appendix D.
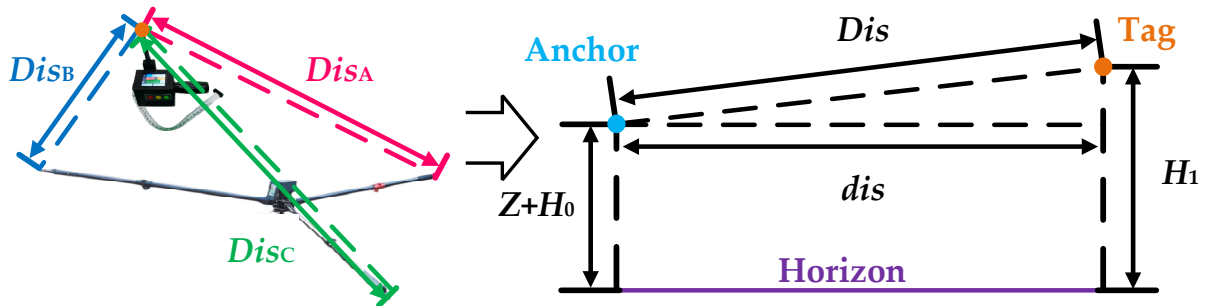

Figure 7. Convert the linear distance between the tag and anchor to the projected distance.

The projection distances dis_A, dis_B, and dis_C can be calculated as follows:

$$\begin{aligned} dis_A &= \sqrt{Dis_A{}^2 - (H1 - H0 - Z_A)^2} \\ dis_B &= \sqrt{Dis_B{}^2 - (H1 - H0 - Z_B)^2} \\ dis_C &= \sqrt{Dis_C{}^2 - (H1 - H0 - Z_C)^2} \end{aligned} \quad (5)$$

where dis_A, dis_B, and dis_C are the projected distances between the tag and Anchor A, Anchor B, and Anchor C, respectively, in the 2D coordinate system; H_0 is the height of the geometry center of three poles of the base station measured by using the altimeter; H_1 is the height of the handheld device measured by using the altimeter.

Although the penetration ability of UWB wireless signals is very strong, in an actual forest survey, the random ranging error may be caused by a thick tree stem, dense bushes, or a human body [7,51–54], resulting in Dis_A, Dis_B, and Dis_C (dis_A, dis_B, and dis_C) that may be slightly longer than the actual distances, and consequently, the three circles for positioning the tag may not intersect at one common point (Figure 8). The received signal strength indication (RSSI) theory [7,52–54] suggests ways to mitigate the effects of signal attenuation on ranging, to improve accuracy and to increase positioning precision [7,53–55].
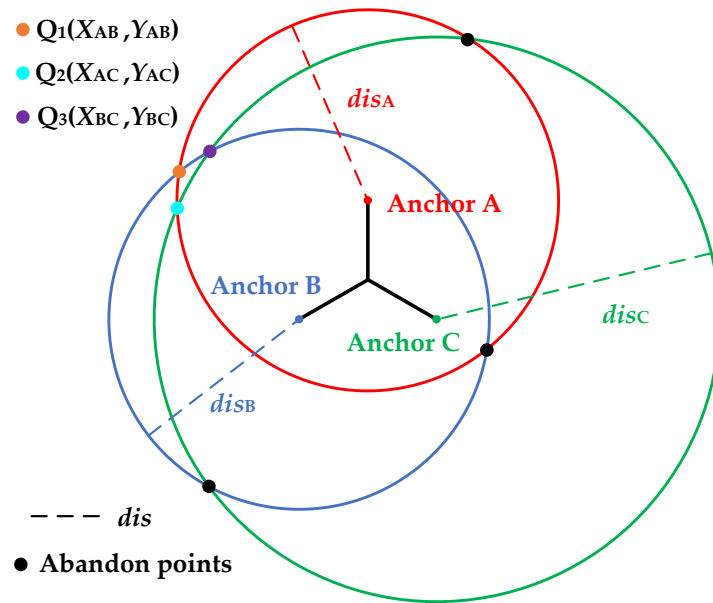

Figure 8. Tree position estimation using trilateration localization theory.

According to the trilateration localization algorithm [53–58], the following equations can be developed:

$$
\begin{cases}
(X_{AB} - X_A)^2 + (Y_{AB} - Y_A)^2 = dis_A{}^2 \\
(X_{AB} - X_B)^2 + (Y_{AB} - Y_B)^2 = dis_A{}^2 \\
(X_{AB} - X_B)^2 + (Y_{AB} - Y_B)^2 = dis_B{}^2 \\
(X_{BC} - X_A{}^2 + (Y_{BC} - Y_A)^2 = dis_B{}^2 \\
(X_{AC} - X_C{}^2 + (Y_{AC} - Y_C)^2 = dis_C{}^2 \\
(X_{BC} - X_C)^2 + (Y_{BC} - Y_C)^2 = dis_C{}^2
\end{cases}
\tag{6}
$$

The coordinates of Q_1 (X_{AB}, Y_{AB}), Q_2 (X_{AC}, Y_{AC}), and Q_3 (X_{BC}, Y_{BC}) can be obtained from Equation (6) by abandoning three other points in the 2D coordinate system (Figure 8). According to the RSSI theory, the above equations can be used to calculate the coordinates of (X, Y) as follows:

$$
\begin{cases}
X = \dfrac{\frac{X_{AB}}{dis_A{}^2+dis_B{}^2} + \frac{X_{AC}}{dis_A{}^2+dis_C{}^2} + \frac{X_{BC}}{dis_B{}^2+dis_C{}^2}}{\frac{1}{dis_A{}^2+dis_B{}^2} + \frac{1}{dis_B{}^2+dis_C{}^2} + \frac{1}{dis_B{}^2+dis_C{}^2}} \\[2em]
Y = \dfrac{\frac{Y_{AB}}{dis_A{}^2 dis_B{}^2} + \frac{Y_{AC}}{dis_A{}^2+dis_C{}^2} + \frac{Y_{BC}}{dis_B{}^2+dis_C{}^2}}{\frac{1}{dis_A{}^2+dis_B{}^2} + \frac{1}{dis_A{}^2+dis_C{}^2} + \frac{1}{dis_B{}^2+dis_C{}^2}}
\end{cases}
\tag{7}
$$

2.2.5. Evaluation of the Accuracy of the Tree DBH and Tree Position

The tree DBH reference value was obtained by measuring the tree DBH using a DBH tape in the 6 plots, and the average was used as the reference tree DBH value for comparison. The accuracy of using the handheld device to measure tree DBH was evaluated by comparing with the reference tree DBH value and by calculating the bias, relative bias,

root mean square error (RMSE), relative RMSE, and mean absolute percent error (MAPE), as defined in the following equations:

$$BIAS = \frac{\sum_{j=1}^{n} (mj - mj\mathrm{r})}{n} \qquad (8)$$

$$relBIAS = \frac{\sum_{j=1}^{n} (mj / mjr - 1)}{n} \times 100\% \qquad (9)$$

$$RMSE = \sqrt{\frac{\sum_{j=1}^{n} (mj - mjr)^2}{n}} \qquad (10)$$

$$relRMSE = \sqrt{\frac{\sum_{j=1}^{n} (mj / mjr - 1)^2}{n}} \times 100\% \qquad (11)$$

where m_j is the *j*-th tree DBH measured using the handheld device in this paper, m_{jr} is the *j*-th tree reference DBH measured using a DBH tape, and n is the number of measured trees.

The reference tree position was measured using a forest compass equipped with a laser distance meter and converted into the OXY plane coordinate system. When measuring the position of a tree, the forest compass was installed at the center point of the plot. The north angle between the stem and north and the horizontal distance from the plot center to the trunk were measured using the forest compass equipped with a laser distance meter, and the results were recorded manually. If the laser distance meter was obscured by other stems or shrubs, we moved the compass to the other reference points with known coordinates near the center point. The reference tree position was calculated from the north angle, horizontal distance, and coordinate of the center point or other point. The bias and RMSE were calculated to reflect the accuracy of the tree position in the x- and y-axis directions, respectively. The errors of the distance (Ed) between the measured and the reference position values were calculated as follows:

$$Ed = \sqrt{(X_j - X_{jr})^2 + (Y_j - Y_{jr})^2} \qquad (12)$$

where X_j and Y_j are the *j*-th tree position estimators in the x-axis and y-axis directions, respectively; X_{jr} and X_{jr} are the *j*-th position reference values in the x-axis and y-axis directions, respectively, of the OXY plane coordinate system.

3. Results

3.1. Evaluation of Tree DBH

The tree DBH measurements, using the presented method, were similar to those measured using a DBH tape (Figure 9), resulting in a bias of 0.05 cm (0.20%) and a RMSE of 0.36 cm (1.45%) across all plots (Table 2). The accuracy of tree DBH for the six plots was high since the bias ranged from approximately −0.04 to 0.10 cm, the relative bias ranged from approximately −0.25% to 0.38%, the RMSE ranged from approximately 0.24 to 0.48 cm, and the relative RMSE ranged from approximately 1.20% to 1.55%. The error for each tree size distributed normally (Figure 10). However, there was a trend, i.e., as the tree DBH increased, more variation in error was observed.
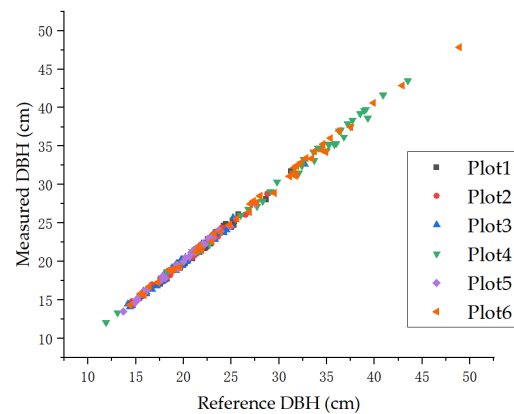
Figure 9. Scatter plot between the measured tree DBH values using the presented method and the reference tree DBHs measured using a DBH tape.

Table 2. Accuracy of the tree DBH measurements obtained using the presented method based on a comparison with the reference DBH obtained from measurements using a DBH tape.

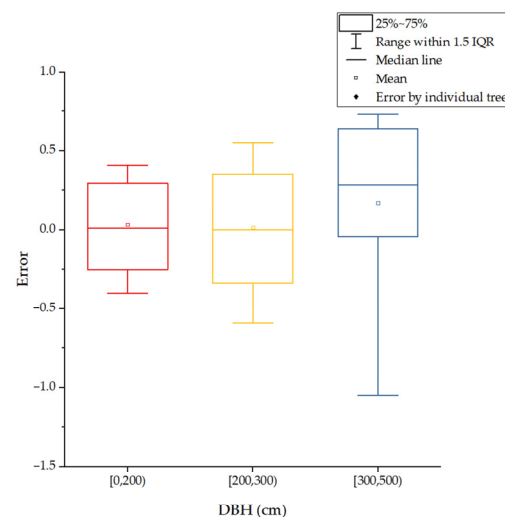| Plot	BIAS (cm)	relBIAS (%)	RMSE (cm)	relRMSE (%)
1	−0.04	−0.25	0.34	1.55
2	0.06	0.28	0.29	1.39
3	0.02	0.14	0.30	1.51
4	0.09	0.28	0.48	1.49
5	0.08	0.38	0.24	1.20
6	0.10	0.36	0.46	1.53
Total	0.05	0.20	0.36	1.45

Figure 10. Distribution of the error in the tree DBH for different tree (DBH) sizes.

3.2. Evaluation of Tree Position

The measured and reference tree positions are given in Figure 11. The bias ranged from approximately −15.92 to 9.92 cm on the x-axis and from −25.90 to 10.88 cm on the y-axis (Table 3). The RMSEs in the x-axis (21.51 cm) and y-axis (22.49 cm) directions were similar (Table 3). Figure 12 presents the errors of the distance (Ed) between the measured and corresponding reference position values by individual tree, ranging from 2.02 to 77.54 cm in the OXY plane. The mean value of the Ed was 27.11 cm, with a standard deviation of 15.30 cm across plots, and ranging from 19.30 to 42.06 cm by plot (Table 4). The RMSE

and average Ed values of Plot 4 and Plot 6 were relatively larger than the other four plots. Therefore, if a plot had a larger mean DBH, the RMSE and Ed were relatively larger.
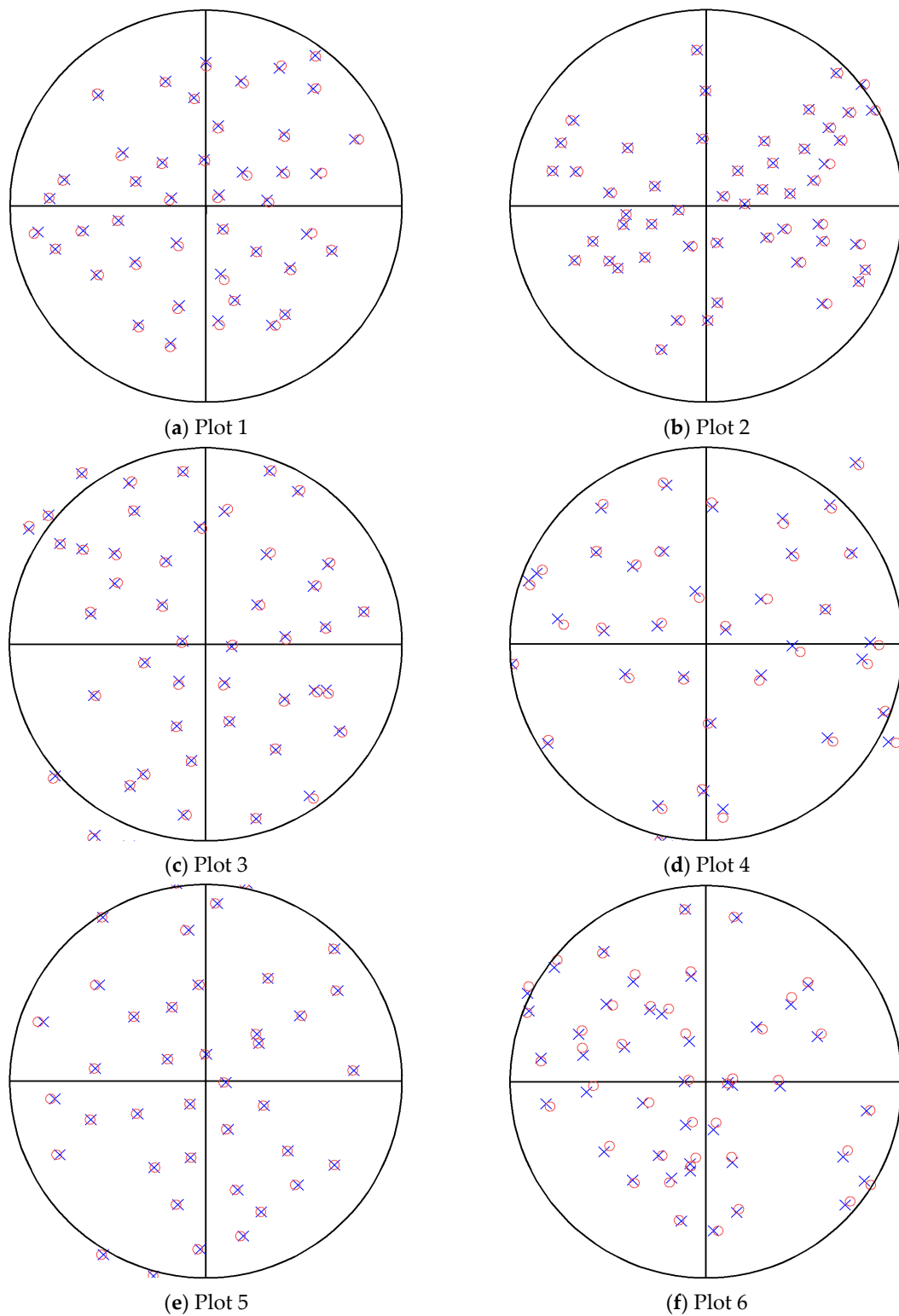

(**a**) Plot 1

(**b**) Plot 2

(**c**) Plot 3

(**d**) Plot 4

(**e**) Plot 5

(**f**) Plot 6

Figure 11. Measured and reference tree positions; (**a**) test plot number 1; (**b**) test plot number 2; (**c**) test plot number 3; (**d**) test plot number 4; (**e**) test plot number 5; (**f**) test plot number 6; the blue crosses represent the measurements; the red circles represent the references.

Table 3. Accuracy in the x- and y-axis directions measured by the presented method.

Plot	X (cm)		Y (cm)	
	BIAS	**RMSE**	**BIAS**	**RMSE**
1	−6.06	17.81	10.88	17.51
2	−10.30	18.01	−7.34	18.94
3	−7.60	15.27	3.99	14.49
4	−14.42	29.40	9.12	27.56
5	9.92	15.63	3.54	15.48
6	−15.92	28.98	−25.90	34.68
Total	−7.63	21.51	2.56	22.49
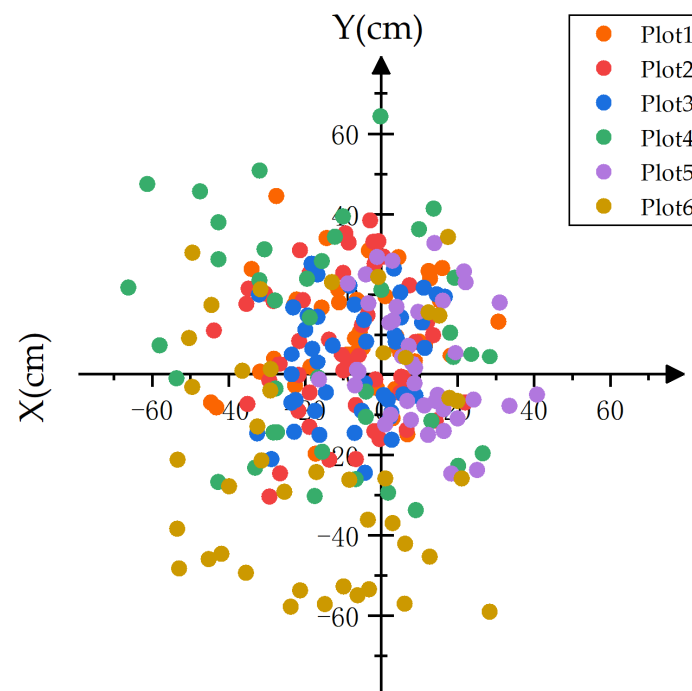
Figure 12. Errors in tree positions measured by the presented method.

Table 4. Summary statistics of the error of the distance between measured and reference points.

Plot	Ed (cm)			
	Mean	**Max**	**Min**	**Std [1]**
1	22.00	52.32	3.61	11.83
2	23.73	45.20	2.02	10.96
3	19.30	37.83	4.88	8.36
4	36.89	77.54	5.85	16.21
5	19.76	41.12	6.01	9.66
6	42.06	71.65	5.46	16.54
Total	27.11	77.54	2.02	15.30

[1] Std, standard deviation.

3.3. Comparing the Efficiency of Different Methods

To evaluate the efficiency of the measurements, the times required for the traditional method and the presented method were recorded. To ensure that the two methods worked in the same order, the trees in the six plots were numbered prior to measurement. Using the traditional method required three people in a group: one person measured tree DBHs using a DBH tape, another person measured the tree positions using a forest compass equipped with a laser distance meter, and the other person manually recorded data with paper and

pen. After the measurements were completed, the data recorded on paper were entered into the computer. The working times of the two methods are shown in Table 5. The results show that the mean measurement times were 20.34 and 48.30 s using the presented method and the traditional method, respectively. Therefore, working efficiency can be increased by more than double using the presented method.

Table 5. Comparison of the efficiency between the traditional method and the presented method.

Method	Number of Surveyors	Number of Trees	Filed Working Time (min)	Office Working Time (min)	Total Time (min)	Mean Time (s)
Traditional method	3	264	191.08	21.43	212.51	48.30
Presented method	1	264	89.52	0	89.52	20.34

4. Discussion

Tree DBH and tree position measurements are important tasks in forest resource surveys. In this study, we reported on a new integrated forest surveying method that can measure tree DBH using a TMR encoder, and tree position using UWB modules and multi-sensors.

The results show that DBH measurements had a 0.05 cm (0.20%) bias and a 0.36 cm (1.45%) RMSE (Table 2), suggesting that the presented method is accurate for measuring tree DBH. The conventional tree DBH measurement method uses a diameter tape or a caliper, data are recorded manually, and it is time-consuming and labor-intensive. Modern tools to measure tree DBH have been developed to improve efficiency. Binot et al. [11] developed an electronic tree measuring fork to measure tree DBH, and the overestimation of tree DBH was generally less than 2%. Liu et al. [29] developed a portable high-precision device for tree diameter measurement using a draw-wire displacement sensor, and the accuracy of this equipment for different tree species reached more than 99.97%. However, these new contact methods could not measure both tree DBH and tree position, and their costs were expensive. Some non-contact methods for measuring tree DBH and tree position simultaneously have been developed. Fan et al. [1] obtained a +0.33 cm bias and a 1.26 cm RMSE for tree DBH measurements using a mobile phone with a TOF camera and SLAM technology. Zhao et al. [23] used a ground photogrammetry method to estimate tree DBH, and reported a rRMSE of the DBH estimates of individual trees that ranged from 3.01 to 6.43%. Liang et al. [56] estimated tree DBH using a multi-single-scan TLS method in forest inventories, and reported a RMSE range from 0.90 to 1.90 cm. However, the tree DBH measurement accuracy of the non-contact methods may have been affected by environmental conditions such as light intensity and stand density. Song et al. [57] presented a handheld device for measuring the DBH of individual trees that used digital cameras and laser ranging, and they reported a 0.636 cm RMSE of individual trees measured. The instruments were also expensive and the microprocessors required high computational capacity, limiting their application in forestry inventory.

Our results also suggest that the presented method can estimate tree positions accurately, with the resulting bias (from −15.92 to 9.92 cm on the x-axis and from −25.90 to 10.88 cm on the y-axis), RMSE (15.27–29.40 cm and 14.49–34.68 cm on the x-axis and the y-axis, respectively), and Ed (27.11 cm) being small. Fan et al. [1] used the SLAM algorithms paired with a TOF camera to estimate tree position and reported an RMSE of 0.12 m, regardless of the axis directions. However, the high accuracy was based on sample plots with no weeds and small shrubs; therefore, application of their method in dense forests needs further verification. Tang et al. [58] used a small-footprint mobile LiDAR to scan a study area, and reported a positioning accuracy better than 0.32 m in two different areas, with expensive and heavy hardware. Zhao et al. [23] also used UWB technology to estimate tree positions, and reported a RMSE range from 0.07 m to 0.16 m. However, their UWB

positioning method required calibration of the four corners of the plot, and each corner was placed with a UWB module. Thus, the method was complex and time-consuming.

In terms of user experience and working efficiency, the traditional methods and newly proposed methods that use a moving terrestrial laser scanner and GNSS require a surveyor to carry more heavy equipment in forest measurements, while the hardware developed in this paper can realize the integration of office and field survey functionalities for recording, uploading, and storing data and has much lower complexity with respect to both time and space. The working efficiency of our method is increased by more than double compared to the traditional method (Table 5).

5. Conclusions

In this paper, we have reported on a new method for forest resource inventory that can measure tree DBH and tree position concurrently by using novel hardware and algorithms. Specifically, we integrated several advanced sensor technologies (TMR encoder, UWB, 3D compass, altimeter, and so on) into the hardware and designed rapid, non-complex, and high-resolution algorithms to improve the measurement accuracy and efficiency. The experimental results have shown that this method can be used to accurately measure tree DBH and tree positions. Additionally, the hardware consisting of a handheld device and a base station equipped with a tripod is inexpensive and easy to use and carry in the field. Nonetheless, we plan to continue to improve the method, in particular, adding the function of tree height measurement.

Appendix A

Table A1. Descriptive statistics of the handheld device's electronic components.

Component	Type	Parameter	Function
TMR encoder	PD-1503-SDI	Bit, 12	DBH measurement
MCU	STC15W4K56S4	Flash, 56 KB	Data processing
UWB module	D-DWM-PG2.5	Resolution, 1 cm and range, 130 m	Distance measurement
SD card	Micro SD	2 GB	Data storage
Bluetooth	JDY-31	Range, 0–15 m	Communication with smartphone
Display	TJC3224T124	320 × 240 pixels	Data display
Battery	ZONGCELL	4000 mAh	Power supply

Appendix B

Table A2. Descriptive statistics of the base station's electronic components.

Component	Type	Parameter	Function
UWB module × 5	D-DWM-PG2.5	Resolution, 1 cm and range, 0–130 m	Distance measurement
3D-compass	DCM250B	Resolution, $0.1°$ Heading range, $0\sim360°$ Heading accuracy, $0.8°$, $1.5°$, $2.0°$, and $3.0°$ (inclined angle $<10°$, $30°$, $40°$, $60°$) Roll and pitch range, $-85°\sim85°$ Roll and pitch accuracy, $0.1°$, $0.2°$, and $0.3°$ (between $\pm15°$, $\pm30°$, $\pm60°$ in range)	Attitude angle measurement
Display	TJC3224T124	320×240 pixels	Data display
Mobile battery	ROMOSS	10000 mAh	Power supply

Appendix C

The internal structure and circuit diagram of the TMR encoder is shown in Figure A1. The wire ports are connected to the power line (Vcc) and ground line (GND), and the digital signal lines (STEP, DIR, and INX). The magnetic shielding shell mainly protects the internal structure and shields the external magnetic field. Internally, the magnetic field change caused by the rotation of the magnet driven by the rotating shaft is detected by the encoder chip. The encoder chip is integrated with two sets of whistle bridges consisting of eight TMR elements ($R_{1\sim8}$); R_1 and R_4 have the same magnetization direction ($180°$) of the pin layer, R_2 and R_3 have the same magnetization direction ($0°$) of the pin layer and are opposite to R_1, R_5 and R_8 have the same magnetization direction ($90°$) of the pin layer and are orthogonal to R_1 and R_4, R_6 and R_7 have the same magnetization direction ($270°$) of the pin layer and are opposite to R_5. The principle of using TMR elements to detect the rotation angle is as follows: When the magnet on the rotating shaft is rotating, the magnetization direction of the free layer follows the magnetic field direction of the magnet, and therefore the resistance of the TMR element changes; the angle detection is achieved by the relationship between the resistance of the TMR element and the relative angle of the magnetization direction between the pin layer and the free layer. Finally, the 2 cosine waves (between A+ and A− and between B+ and B−) are converted to digital signals by means of filters, analog-to-digital converters, and microprocessor processing.
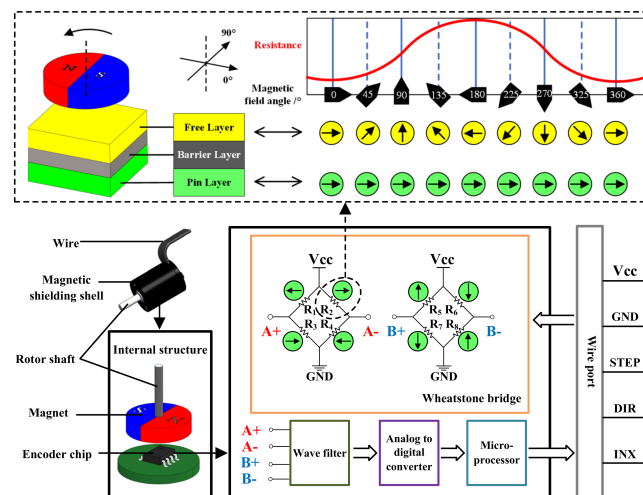

Figure A1. The internal structure and circuit diagram of TMR encoder.

Appendix D

Figure A2 presents an example of calculating the distance (*Dis*) between two UWB modules (Tag and Anchor) using double-sided two-way ranging (DS-TWR) [7]. The *Dis* between Tag and Anchor can be calculated as follows:

$$Dis = c \times T_{pp} = c \times \frac{T_{rd1} \times T_{rd2} - T_{rp1} \times T_{rp2}}{T_{rd1} + T_{rd2} + T_{rp1} + T_{rp2}} \tag{A1}$$
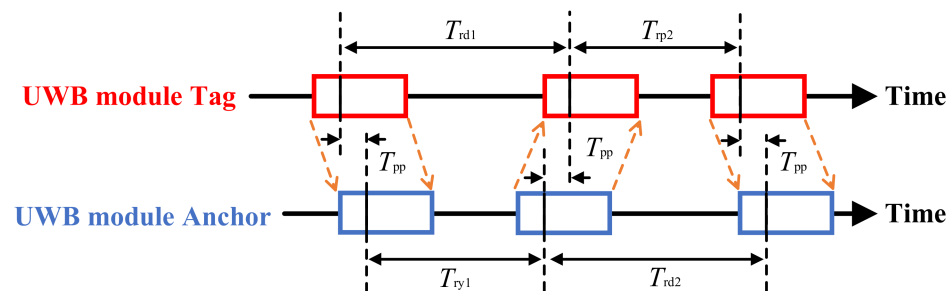

Figure A2. Double-sided Two-way ranging.

In figure, where T_{pp} is the time of the wireless signal propagation in the air; c is the speed of light in the air; time is the time axis; the times T_{rd1}, T_{rd2}, T_{ry1} and T_{ry2} are measured independently by Tag and Anchor using their respective local clocks; T_{rd1} is the total time of Tag sending and receiving pulses in the first round of communication; T_{ry1} is the reply time for Anchor in the first round of communication; T_{rd2} is the total time of Anchor sending and receiving pulses in the second round of communication; T_{ry2} is the reply time for Tag in the second round of communication [7].

References

1. Fan, Y.; Feng, Z.; Mannan, A.; Khan, T.U.; Shen, C.; Saeed, S. Estimating Tree Position, Diameter at Breast Height, and Tree Height in Real-Time Using a Mobile Phone with RGB-D SLAM. *Remote Sens.* **2018**, *10*, 1845. [CrossRef]
2. Macdicken, K.G. Global Forest Resources Assessment 2015: What, why and how? *For. Ecol. Manag.* **2015**, *352*, 3–8. [CrossRef]
3. Trumbore, S.; Brando, P.; Hartmann, H. Forest health and global change. *Science* **2015**, *349*, 814–818. [CrossRef] [PubMed]
4. Tubiello, F.N.; Salvatore, M.; Ferrara, A.F.; House, J.; Federici, S.; Rossi, S.; Biancalani, R.; Condor Golec, R.D.; Jacobs, H.; Flammini, A.; et al. The contribution of agriculture, forestry and other land use activities to global warming, 1990–2012. *Glob. Chang. Biol.* **2015**, *21*, 2655–2660. [CrossRef]
5. Zhang, L.; Bi, H.; Cheng, P.; Davis, C.J. Modeling spatial variation in tree diameter—Height relationships. *For. Ecol. Manag.* **2004**, *189*, 317–329. [CrossRef]
6. Millar, C.I.; Stephenson, N.L. Temperate forest health in an era of emerging megadisturbance. *Science* **2015**, *349*, 823–826. [CrossRef]
7. Sun, L.; Fang, L.; Weng, Y.; Zheng, S. An Integrated Method for Coding Trees, Measuring Tree Diameter, and Estimating Tree Positions. *Sensors* **2020**, *20*, 144. [CrossRef]
8. Bauwens, S.; Fayolle, A.; Gourlet-Fleury, S.; Ndjele, L.M.; Mengal, C.; Lejeune, P. Terrestrial photogrammetry: A non-destructive method for modelling irregularly shaped tropical tree trunks. *Methods Ecol. Evol.* **2017**, *8*, 460–471. [CrossRef]
9. Kangas, A.; Maltamo, M. *Forest Inventory: Methodology and Applications*; Springer Science & Business Media: Dordrecht, The Netherlands, 2006.
10. Luoma, V.; Saarinen, N.; Wulder, M.A.; White, J.C.; Vastaranta, M.; Holopainen, M.; Hyyppä, J. Assessing Precision in Conventional Field Measurements of Individual Tree Attributes. *Forests* **2017**, *8*, 38. [CrossRef]
11. Binot, J.-M.; Pothier, D.; Lebel, J. Comparison of relative accuracy and time requirement between the caliper, the diameter tape and an electronic tree measuring fork. *For. Chron.* **1995**, *71*, 197–200. [CrossRef]
12. Michael, K.; Steen, S.M.; Marco, M. *Sampling Methods, Remote Sensing and GISMultiresourceForest Inventory*; Spring-Verlag Berlin Heidelberge: Berlin, Germany, 2006.
13. Wu, X.; Zhou, S.; Xu, A.; Bin, C. Passive measurement method of tree diameter at breast height using a smartphone. *Comput. Electron. Agric.* **2019**, *163*, 104875. [CrossRef]
14. Tomaštík, J.; Saloň, Š.; Tunák, D.; Chudý, F.; Kardoš, M. Tango in forests—An initial experience of the use of the new Google technology in connection with forest inventory tasks. *Comput. Electron. Agric.* **2017**, *141*, 109–117. [CrossRef]

15. Vastaranta, M.; Melkas, T.; Holopainen, M.; Kaartinen, H.; Hyyppae, J.; Hyyppae, H. Laser-based field measurements in tree-level forest data acquisition. *Photogramm. J. Finl.* **2009**, *21*, 51–61.

16. Wang, Z.; Lu, X.; An, F.; Zhou, L.; Wang, X.; Wang, Z.; Zhang, H.; Yun, T. Integrating Real Tree Skeleton Reconstruction Based on Partial Computational Virtual Measurement (CVM) with Actual Forest Scenario Rendering: A Solid Step Forward for the Realization of the Digital Twins of Trees and Forests. *Remote Sens.* **2022**, *14*, 6041. [CrossRef]

17. Zou, W.; Jing, W.; Chen, G.; Lu, Y.; Song, H. A Survey of Big Data Analytics for Smart Forestry. *IEEE Access* **2019**, *7*, 46621–46636. [CrossRef]

18. Wang, Z.; Shen, Y.-J.; Zhang, X.; Zhao, Y.; Schmullius, C. Processing Point Clouds Using Simulated Physical Processes as Replacements of Conventional Mathematically Based Procedures: A Theoretical Virtual Measurement for Stem Volume. *Remote Sens.* **2021**, *13*, 4627. [CrossRef]

19. Torresan, C.; Garzón, M.B.; O'Grady, M.; Robson, T.M.; Picchi, G.; Panzacchi, P.; Tomelleri, E.; Smith, M.; Marshall, J.; Wingate, L.; et al. A new generation of sensors and monitoring tools to support climate-smart forestry practices. *Can. J. For. Res.* **2021**, *51*, 1751–1765. [CrossRef]

20. Barrett, F.; McRoberts, R.E.; Tomppo, E.; Cienciala, E.; Waser, L.T. A questionnaire-based review of the operational use of remotely sensed data by national forest inventories. *Remote Sens. Environ.* **2016**, *174*, 279–289. [CrossRef]

21. Gougherty, A.V.; Keller, S.R.; Kruger, A.; Stylinski, C.D.; Elmore, A.J.; Fitzpatrick, M.C. Estimating tree phenology from high frequency tree movement data. *Agric. For. Meteorol.* **2018**, *263*, 217–224. [CrossRef]

22. Yao, Q.; Wang, J.; Zhang, J.; Xiong, N. Error Analysis of Measuring the Diameter, Tree Height, and Volume of Standing Tree Using Electronic Theodolite. *Sustainability* **2022**, *14*, 6950. [CrossRef]

23. Zhao, Z.; Feng, Z.; Liu, J.; Wang, Y. Development and Testing of a New UWB Positioning Measurement Tool to Assist in Forest Surveys. *Sustainability* **2022**, *14*, 17042. [CrossRef]

24. Clark, N.; Wynne, R.; Schmoldt, D. A review of past research on dendrometers. *For. Sci.* **2000**, *46*, 570–576.

25. Mokroš, M.; Výbošťok, J.; Tomaštík, J.; Grznárová, A.; Valent, P.; Slavík, M.; Merganič, J. High Precision Individual Tree Diameter and Perimeter Estimation from Close-Range Photogrammetry. *Forests* **2018**, *9*, 696. [CrossRef]

26. Surový, P.; Yoshimoto, A.; Panagiotidis, D. Accuracy of reconstruction of the tree stem surface using terrestrial close-range photogrammetry. *Remote Sens.* **2016**, *8*, 123. [CrossRef]

27. Jingchen, L.; Zhongke, F.; Yongxiang, F. Automatic measurement of DBH with electronic bar. *Trans. Chin. Soc. Agric. Mach.* **2017**, *48*, 1–9.

28. Sun, L.; Fang, L.; Tang, L.; Liu, J. Developing portable system for measuring diameter at breast height. *J. Beijing For. Univ.* **2018**, *40*, 82–89.

29. Liu, H.; Feng, Z.; Hu, N.; Liu, J.; Yu, X. Design and experiment of portable high precision equipment for tree diameter measurement. *Trans. Chin. Soc. Agric. Mach.* **2018**, *49*, 189–194.

30. Sun, L.; Fang, L.; Fang, Y.; Weng, Y.; Lou, X. Development of dbh measurement device using capacitive gate sensor. *Chin. J. Sens. Actuators* **2019**, *32*, 1435–1442.

31. Liang, X.; Litkey, P.; Hyyppa, J.; Kaartinen, H.; Vastaranta, M.; Holopainen, M. Automatic stem mapping using single-scan terrestrial laser scanning. *IEEE Trans. Geosci. Remote Sens.* **2012**, *50*, 661–670. [CrossRef]

32. Béland, M.; Widlowski, J.-L.; Fournier, R.A.; Côté, J.-F.; Verstraete, M.M. Estimating leaf area distribution in savanna trees from terrestrial LiDAR measurements. *Agric. For. Meteorol.* **2011**, *151*, 1252–1266. [CrossRef]

33. Srinivasan, S.; Popescu, S.C.; Eriksson, M.; Sheridan, R.D.; Ku, N.-W. Terrestrial laser scanning as an effective tool to retrieve tree level height, crown width, and stem diameter. *Remote Sens.* **2015**, *7*, 1877–1896. [CrossRef]

34. Xie, Y.; Yang, T.; Wang, X.; Chen, X.; Pang, S.; Hu, J.; Wang, A.; Chen, L.; Shen, Z. Applying a Portable Backpack Lidar to Measure and Locate Trees in a Nature Forest Plot: Accuracy and Error Analyses. *Remote Sens.* **2022**, *14*, 1806. [CrossRef]

35. Labelle, E.R.; Heppelmann, J.B.; Borchert, H. Application of Terrestrial Laser Scanner to Evaluate the Influence of Root Collar Geometry on Stump Height after Mechanized Forest Operations. *Forests* **2018**, *9*, 709. [CrossRef]

36. Lian, Y.; Feng, Z.; Huai, Y.; Lu, H.; Chen, S.; Li, N. Terrestrial Videogrammetry for Deriving Key Forest Inventory Data: A Case Study in Plantation. *Remote Sens.* **2021**, *13*, 3138. [CrossRef]

37. Hyyppä, J.; Virtanen, J.-P.; Jaakkola, A.; Yu, X.; Hyyppä, H.; Liang, X. Feasibility of Google Tango and Kinect for crowdsourcing forestry information. *Forests* **2017**, *9*, 6. [CrossRef]

38. Prusty, S.; Sahoo, S. Detection of forest fire by using gsm & gps technology. *Int. J. Intell. Comput. Appl. Sci.* **2017**, *5*, 2322–2353.

39. Keefe, F.R.; Wempe, M.A.; Becker, M.R.; Zimbelman, G.E.; Nagler, S.E.; Gilbert, L.S.; Caudill, C.C. Positioning methods and the use of location and activity data in forests. *Forests* **2019**, *10*, 458. [CrossRef]

40. Pau, L.F.; Klamerus-Iwan, A.; Kormanek, M.; Goł, J.; Owsiak, K. Robotic forest harvesting process using gnss satellite positioning data: Effects of gnss inaccuracies in forest environments. In *Electronic Journal of Polish Agricultural Universities*; Electronic Journal of Polish Agricultural Universities: Krakow, Poland, 2016.

41. Feng, T.; Chen, S.; Feng, Z.; Shen, C.; Tian, Y. Effects of Canopy and Multi-Epoch Observations on Single-Point Positioning Errors of a GNSS in Coniferous and Broadleaved Forests. *Remote Sens.* **2021**, *13*, 2325. [CrossRef]

42. Agarwal, R.; Bhatti, G.; Singh, R.R.; Indragandhi, V.; Suresh, V.; Jasinska, L.; Leonowicz, Z. Intelligent Fault Detection in Hall-Effect Rotary Encoders for Industry 4.0 Applications. *Electronics* **2022**, *11*, 3633. [CrossRef]

43. Meng, B.; Wang, Y.; Sun, W.; Yuan, X. A Novel Diagnosis Method for a Hall Plates-Based Rotary Encoder with a Magnetic Concentrator. *Sensors* **2014**, *14*, 13980–13998. [CrossRef] [PubMed]

44. Wang, S.; Wu, Z.; Peng, D.; Chen, S.; Zhang, Z.; Liu, S. Sensing Mechanism of a Rotary Magnetic Encoder Based on Time Grating. *IEEE Sens. J.* **2018**, *18*, 3677–3683. [CrossRef]

45. Tomoya, N.; Hirofumi, S.; Prabhanjan, D.K.; Hitoshi, I.; Yuya, S. Tunnel magnetoresistance sensors with symmetric resistance-field response and noise properties under AC magnetic field modulation. *Appl. Phys. Lett.* **2022**, *121*, 19.

46. Palacín, J.; Martínez, D. Improving the Angular Velocity Measured with a Low-Cost Magnetic Rotary Encoder Attached to a Brushed DC Motor by Compensating Magnet and Hall-Effect Sensor Misalignments. *Sensors* **2021**, *21*, 4763. [CrossRef]

47. Linhao, S.; Zhongke, F.; Jueying, S.; Yakui, S.; Dangui, L.; Tiantian, M. Development and experiment of the portable high precision measurement device for tree DBH. *Trans. Chin. Soc. Agric. Mach.* **2022**, *38*, 31–41.

48. Wisiak, K.; Jakić, M.; Hartlieb, P. Application of Ultra-Wide Band Sensors in Mining. *Sensors* **2023**, *23*, 300. [CrossRef] [PubMed]

49. Matteo, R.; Samuel, V.D.V.; Heidi, S.; De Poorter, E. Analysis of the scalability of UWB indoor localization Solutions for High User Densities. *Sensors* **2018**, *18*, 1875.

50. Xiaoping, H.; Fei, W.; Jian, Z.; Hu, Z.; Jin, J. A posture recognition method based on indoor positioning technology. *Sensors* **2019**, *19*, 1464.

51. Juri, S.; Volker, S.; Norbert, S.; Arensa, M.; Hugentobler, U. Decawave UWB clock drift correction and powerself-calibration. *Sensors* **2019**, *19*, 2942.

52. Gao, H.; Li, X. Tightly-Coupled Vehicle Positioning Method at Intersections Aided by UWB. *Sensors* **2019**, *19*, 2867. [CrossRef] [PubMed]

53. Zabalegui, P.; De Miguel, G.; Mendizabal, J.; Adin, I. Innovation-Based Fault Detection and Exclusion Applied to Ultra-WideBand Augmented Urban GNSS Navigation. *Remote Sens.* **2023**, *15*, 99. [CrossRef]

54. Yuan, F.; Chen, S.; Fang, L.; Zheng, S.; Liu, Y.; Ren, J. A Method to Locate Tree Positions Using Ultrawideband Technology. *J. Sens.* **2021**, *2021*, 5539302. [CrossRef]

55. Zhu, X.; Feng, Y. RSSI-based algorithm for indoor localization. *Commun. Netw.* **2013**, *5*, 37–42. [CrossRef]

56. Liang, X.; Hyyppä, J. Automatic stem mapping by merging several terrestrial laser scans at the feature and decision levels. *Sensors* **2013**, *13*, 1614–1634. [CrossRef]

57. Song, C.; Yang, B.; Zhang, L.; Wu, D. A handheld device for measuring the diameter at breast height of individual trees using laser ranging and deep-learning based image recognition. *Plant Methods* **2021**, *17*, 67. [CrossRef] [PubMed]

58. Tang, J.; Chen, Y.; Kukko, A.; Kaartinen, H.; Jaakkola, A.; Khoramshahi, E.; Hakala, T.; Hyyppä, J.; Holopainen, M.; Hyyppä, H. SLAM-Aided Stem Mapping for Forest Inventory with Small-Footprint Mobile LiDAR. *Forests* **2015**, *6*, 4588–4606. [CrossRef]